
Article:
Thermou, G.E., Papanikolaou, V.K. and Hajirasouliha, I. orcid.org/0000-0003-2597-8200 (2021) Structural performance of RC columns retrofitted with steel-reinforced grout jackets under combined axial and lateral loading. Engineering Structures, 245. 112946. ISSN 0141-0296

https://doi.org/10.1016/j.engstruct.2021.112946

Structural Performance of RC Columns Retrofitted with Steel-Reinforced Grout Jackets Under Combined Axial and Lateral Loading

G.E Thermou[1*], V.K. Papanikolaou[2], I. Hajirasouliha[3]

[1] Assistant Professor in Structural Engineering, Dept. of Civil Engineering, The University of Nottingham, NG7 2RD, Nottingham, UK

[2] Assistant Professor, Aristotle University of Thessaloniki, School of Civil Engineering, 54124, Thessaloniki, Greece

[3] Senior Lecturer, Civil and Structural Engineering Department, The University of Sheffield, S1 3JD, Sheffield, UK

Abstract: The effectiveness of steel-reinforced grout (SRG) jacketing in improving the structural performance of deficient reinforced concrete (RC) columns is experimentally investigated in this study. Four full-scale cantilever columns were designed following the old construction practice (pre-1970s) in southern Europe. Due to lack of adequate seismic detailing, the columns were susceptible to buckling failure when subjected to combined axial loading and cyclic lateral displacement reversals, simulating seismic loading. Three alternative SRG jacketing configurations were applied differing in the number of layers and density of the Ultra High Tensile Strength Steel (UHTSS) textile. The test results demonstrated the efficiency of SRG jacketing to modify the response of the columns with poor detailing from brittle to ductile by substantially improving their overall structural performance. Finally, code formulations were used to assess the performance of the SRG jacketed columns.

Keywords: Concrete; columns; strengthening; retrofitting; jackets; ductility; buckling; SRG; FRCM.

[*] Corresponding author, tel: +44 (0) 115 7487229, georgia.thermou@nottingham.ac.uk

1. Introduction

Most reinforced concrete (RC) buildings in southern Europe were built in the first half of the 20th century to carry only gravity loads, by implementing the allowable stress design philosophy which did not allow any control of the failure mode and the corresponding deformation capacity of the individual members [1]. Non-uniform distribution of stiffness and/or mass along the height of the building, poor material quality, and insufficient reinforcement detailing, are some of the main deficiencies that substantially increase the vulnerability of the existing building inventory when exposed to natural hazards, such as earthquakes.

Inadequate confinement has proven detrimental for the integrity of old-type buildings under seismic excitations (Fig. 1). Cyclic inelastic deformation reversals have a severe impact on both strength and deformation capacity of structural members due to the degradation of mechanisms such as concrete in tension (diagonal tension failure) and steel in compression (longitudinal steel buckling) [2]. Typical RC column construction detailing practice till the early 1980s comprised longitudinal reinforcement with bar diameter ranging from 12 mm to 20 mm and open (i.e. anchored with 90° hooks in the ends) stirrups of 6 mm (rarely 8 mm) diameter placed at distances from 200 mm to 600 mm (Fig. 1). Due to the large unsupported length of the longitudinal bars, premature buckling is the anticipated mode of failure for these elements, limiting their compression strain capacity.

In case of old type detailing columns, the bar slenderness ratio s/D_b (s is the stirrup spacing and D_b is the bar diameter of the longitudinal reinforcement), which reflects the stability of compression reinforcing bars supported laterally by stirrups, is generally between 10 and 50 [1]. Based on the work of previous researchers [3-6], for $s/D_b < 6$ and bars with significant strain hardening, axial load-carrying capacity is greatly enhanced beyond the yielding load, thus

inelastic buckling of reinforcing steel bars is expected to occur. For $s/D_b > 10$, the compression reinforcing bars may undergo elastic buckling prior to yielding [7-8].

Fig. 1. Damage in RC columns due to old-type detailing (photos are taken by the authors).

In columns with sparse confinement reinforcement, sideways buckling is the usual form of compression reinforcement failure due to lateral shear distortion of the member in the plastic hinge regions (Fig. 1). An effective way to mitigate buckling of steel reinforcement in the regions of high compression strain demands is by wrapping the column ends externally. The provided confinement allows the concrete in compression to considerably increase its strain capacity. If the strain capacity of the confined concrete is higher than the critical strain at the onset of reinforcement buckling, redistribution between the compressed bars at incipient buckling and the encased concrete is possible, thereby postponing buckling to occur at a higher strain level [9, 10].

Various jacketing techniques have been developed to provide external confinement to substandard RC columns, including Fiber Reinforced Polymer (FRP) [e.g. 11-15] and Textile Reinforced Mortar (TRM) jacketing [e.g. 16-18], Post-Tensioned Metal Straps (PTMS) [e.g. 19], ferrocement jacketing [e.g. 20], welded wire mesh jacketing [e.g. 21], shape memory spirals [e.g. 22], fiber reinforced concrete jacketing [e.g. 23] and ultra high performance-fiber reinforced cementitious composites (UHP-FRCC) jacketing [e.g. 24, 25]. The Steel-Reinforced

Grout (SRG) jacketing was used in a pilot study in 2007 by Thermou and Pantazopoulou [26] for the seismic retrofitting of three pre-damaged 1:2 scaled columns with poor detailing. Two of the columns had failed in shear and the third one in a shear/buckling mixed mode of failure. The single-layered SRG jackets with density 1.85 cords/cm substantially modified the behavior of the retrofitted specimens by altering the modes of failure observed in the pre-damage state. The retrofitted specimens increased both their strength and deformation capacity. In a more recent study [27], SRG jacketing was applied to 1:2 scaled lightly reinforced columns which were susceptible to rebar buckling failure with the compression reinforcing bars losing their stability prior or close to yielding. Single-layered SRG jackets with textile density of 1 and 2 cords/cm managed to increase the compressive strain ductility by 100 % and thus delaying bar buckling and allowing the columns to improve their strength and strain capacity.

For the first time, this paper aims to study the effectiveness of SRG jacketing in delaying bar buckling of full-scale columns representative of the old construction practice when subjected to combined axial loading and cyclic lateral displacement reversals, simulating seismic loading. Three alternative SRG jacketing schemes were applied to three full-scale cantilever columns, whereas the fourth column served as the control specimen. Parameters of study were the density of the textile (1.57 and 4.72 cords/cm) and the number of layers (1 and 2). The test results demonstrated the efficiency of SRG jacketing at preventing the brittle failure mode and substantially improving the structural performance of old-type RC columns. Code formulations, which rely on the design philosophy of FRP design, were used to assess the strength and deformation capacity of the SRG jacketed columns.

2. Experimental program

2.1 Test specimens and parameters of investigation

Four identical reinforced concrete (RC) columns representative of the pre-1970s old-type detailing in southern Europe were tested under reversed cyclic loading simulating earthquake effects. The cantilever columns, constructed at full-scale, were typical building columns extending from column mid-height between floors to the beam-column connection. The columns were designed by following the provisions of the first Greek seismic code introduced in 1959 [28] and were all susceptible to shear-buckling failure. Fig. 2 shows the geometry and reinforcement details of the specimens. All columns had a 250 mm square cross section and a shear span length, L_v = 1640 mm. The longitudinal reinforcement comprised eight 16 mm diameter ribbed longitudinal bars equally distributed throughout the cross section with 15 mm concrete cover. The longitudinal bars were well-anchored in the heavily reinforced footing. The shear reinforcing bars consisted of 6 mm diameter smooth bars with their ends bent at 90°, spaced uniformly at 250 mm centers up to 1500 mm. The stirrup spacing to longitudinal bar diameter ratio was selected to be high (s/D_b = 250/16 = 15.6) complying with old type detailing requirements of that era. In the column heads extending at the upper 320 mm, 8 mm ribbed stirrups anchored with 135° hooks at each end spaced at 60 mm were placed. This region was well-confined as to be protected from possible cracks due to the application of the horizontal and axial loads during testing.

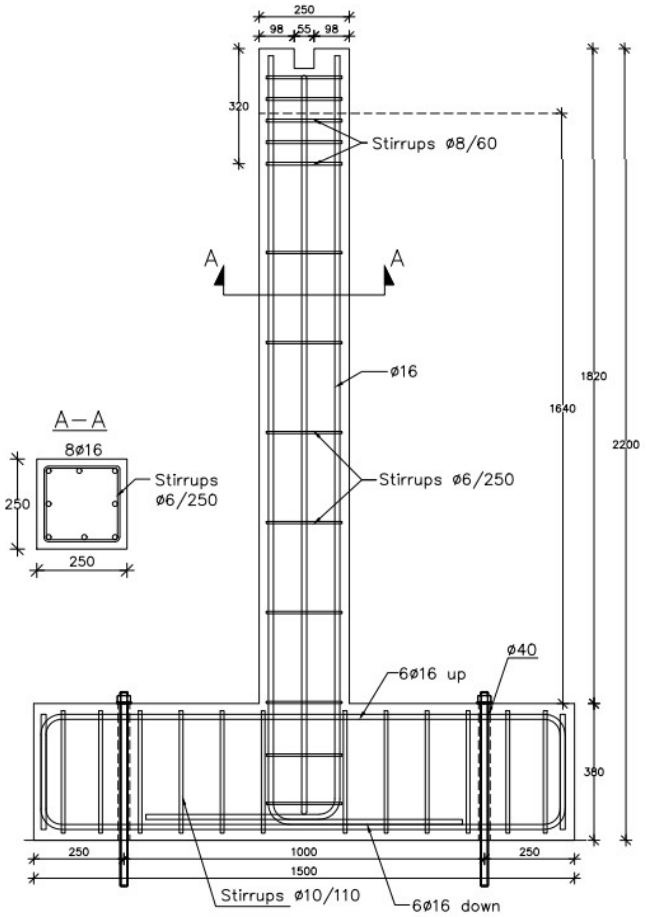

Fig. 2. Column geometry and reinforcement details of the cantilever columns (dimensions in mm).

Three of the columns were strengthened by applying Steel-Reinforced Grout (SRG) jackets whereas one column served as the control specimen. SRG jackets were applied up to a height equal to 1.2 m (Fig. 3). With the width of the role being 30 cm, four regions were identified for the application of the SRG jackets as shown in Fig. 3. To prevent direct loading of the jacket, 1 cm gap was left between the foundation and the steel textile (Fig. 3). Three alternative SRG jacketing schemes were applied, while the parameters of investigation were the density of the textile (i.e. the distance between successive cords) and the number of layers. In this study, the 1.57 and the 4.72 cords/cm densities (or 4 and 12 cords/in, respectively, Figs. 3b, 3c) were used and the number of layers was 1 or 2 (see Table 1). The alternative SRG jacketing schemes were applied in the critical region of the columns, which was considered equal to 60 cm (Regions 1

and 2 in Fig. 3a). Single-layered SRG jackets of 1.57 cords/cm density were applied at the end of the critical zone and up to 120 cm (Regions 3 and 4 in Fig. 3a).

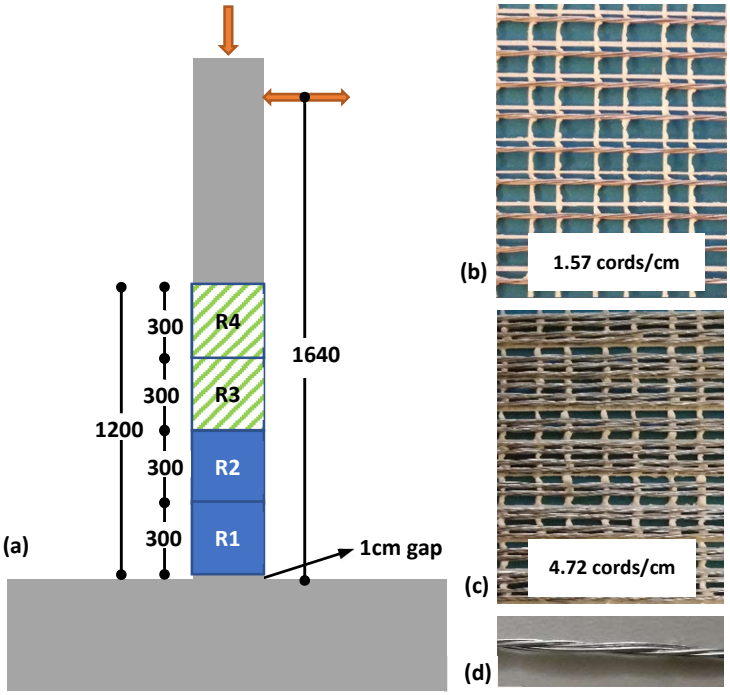

Fig. 3. (a) Retrofitted regions of the columns (dimensions in mm); (b), (c) Densities of the Ultra High Tensile Strength Steel (UHTSS) used in this study; (d) Structure of a single 3X2 steel cord.

As mentioned before, the key parameters of investigation were the density of the Ultra-High Tensile Strength Steel (UHTSS) textile (1.57 and 4.72 cords/cm) and the number of applied SRG layers (one and two). The details of all test specimens are given in Table 1. Column C represents the control specimen. Columns SRG1 and SRG2 correspond to the case that one and two layers of the 1.57 cords/cm textile were applied, respectively. In case of the SRG3 column two layers of the denser textile (4.72 cords/cm) were applied.

Table 1. Details of the tested columns

Column	f_{co} (MPa)	Standard Deviation	SRG jacketing					
			Region 1		Region 2		Region 3 & 4	
			Layer	Density cords/cm	Layer	Density cords/cm	Layer	Density cords/cm
C	24.0	0.33	-	-	-	-	-	-
SRG1	23.2	2.99	1	1.57	1	1.57	1	1.57
SRG2	22.6	1.60	2	1.57	2	1.57	1	1.57
SRG3	21.3	1.31	2	4.72	2	4.72	1	1.57

2.2 Material Properties

Concrete: The four columns were casted in four different batches. The average compressive strength, f_{co}, for each batch at the day of the test was obtained from three standard cylinders (150×300 mm) as presented in Table 1.

Reinforcement Steel: The longitudinal reinforcement comprised 16 mm diameter ribbed bars which had a yield stress of f_y = 550 MPa and ultimate stress f_u = 620 MPa corresponding to StIIIb used for seismic applications in the 1970s. The 6 mm diameter smooth bar reinforcement used for the stirrups had a yield stress of f_{yw} = 360 MPa and ultimate stress of f_{uw} = 470 MPa corresponding to StI. This type of reinforcement was used extensively for shear reinforcement at the time. The mechanical properties of the reinforcement steel were obtained from standard tensile tests.

Ultra-High Tensile Strength Steel (UHTSS): The structure of the high strength steel cord 3X2 corresponds to five individual wires twisted together (three straight filaments wrapped by two filaments at a high twist angle, Fig. 3d). The geometrical and mechanical properties of a single cord 3X2 (as provided by the manufacturer) appear in Table 2. The 3X2 textile is a unidirectional sheet made of ultra-high strength galvanized steel micro-cords, fixed to a fiberglass micromesh to facilitate installation. The textile density (i.e. the density between successive cords) was 1.57 and 4.72 cords/cm, respectively, corresponding to an equivalent thickness per unit width for a single layer of steel textile, t_{SRG}, equal to 0.084 and 0.254 mm, respectively. The axial stiffness of the textile, K_{SRG} (= $A_{SRG}\cdot E_{SRG}$), which is directly related to the density of the textile, was calculated equal to 15960 and 48260 N/mm for the 1.57 and the 4.72 cords/cm textiles, respectively (these figures should be doubled for the two-layered jackets).

Mortar: A commercial geo-mortar with a crystalline reaction geobinder base and a very low petrochemical polymer content and free from organic fibers was used in this study. The

component mortar was utilized as the substrate material applied to the concrete surface of the specimens, the bonding material between the applied layers of the steel textile and as a final cover. According to the technical data sheet, the appearance of the mortar is powder with a volumetric mass 1260 Kg/m3. The aggregate mineral content is silicate – carbonate and it has a grading 0-0.5mm. The mixing water is 5.11 for 25kg bag. The mechanical properties of the mortar at 28 days according to the manufacturer are provided in Table 3.

Table 2. Geometrical and mechanical properties of single cords as provided by the manufacturer

Cord type	Cord diameter (mm)	Cord area (mm^2)	Break load (N)	Tensile strength f_{fu} (MPa)	Strain to failure ε_{fu} (mm/mm)	Elastic modulus E_{SRG} (MPa)
3X2	0.827	0.538	1506	2800	0.015	190000

Table 3. Mechanical properties of the mortar at 28 days as provided by the manufacturer

Mortar	Modulus of elasticity E_m (MPa)	Flexural strength f_{mf} (MPa)	Compressive strength f_{mc} (MPa)	Adhesive bond f_{mb} (MPa)
	20000	8	50	2

2.3 Fabrication of the SRG jackets

The first step involved in the preparation of the steel textiles is to cut them into the desired lengths and then bend them at right angles as to facilitate their application procedure (see Fig. 4a). The overlap length selected for both single- and double-layered jackets covered two full sides according to previous related studies [29-32] (Fig. 4b). For each of the four regions defined along the height of the columns a different piece of textile was utilized (Fig. 3a, Table 1). The concrete substrate was roughened to enhance the bond between the substrate and the mortar (Fig. 4c). A 3 mm thickness cementitious mortar was applied on the concrete surfaces that had been previously cleaned and saturated (Fig. 4d). Then, the textile was placed by applying pressure manually for the grout to be squeezed out between the steel textile (Fig. 4e). This is a key stage for the success of the SRG jacketing method as the steel cords should be fully embedded in the cementitious matrix. After one or two full wraps of the steel textile, the

remaining length was lapped over the lateral surface. A final coat of the cementitious grout was applied to the exposed surface. The jacketed columns were wrapped for a week with wet hessian cloth and then left to dry to room temperature which ranged between 20-25^{0}C. It is worth mentioning that the application of the 4.72 cords/cm two-layered jacket (SRG3 column) imposed difficulties due to the high stiffness of the textile (high density). Achieving a good fit of the second layer of the textile at the corners of the column was challenging. The effect on the geometric dimensions of the jacketed specimens was small. The total thickness of the SRG jacket was between 7 to 10 mm for one- and two-layered jackets.

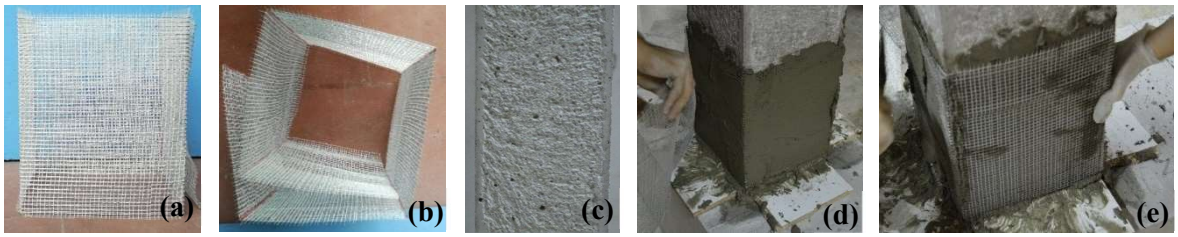

Fig. 4. Steps of the fabrication of the SRG jackets

2.4 Test setup, instrumentation, and cyclic loading protocol

The columns were subjected to cyclic uniaxial bending and simultaneous compressive axial load. The full experimental set-up is shown in Fig. 5a. The columns were anchored to the strong floor via prestressed rods passing through the columns' foundation. The vertical actuator operated in force-control mode. The horizontal actuator was located at a height of 2.04 m from the strong floor and applied a quasi-static cyclic load, operating in external displacement-control mode for guaranteed response accuracy. An external draw wire sensor was placed at height equal to 2.04 m from the strong floor for implementing the closed-loop displacement control (Fig 5b). Both actuators were anchored against a stiff reaction frame.

A reversed cyclic lateral loading of 1 mm/s displacement rate (0.061 %/s drift) was applied with increasing drift levels under a constant normalized axial load equal to 20 % ($\nu = N/A_g f_{co}$; where N is the applied axial load, A_g is the cross-section area and f_{co} is the concrete compressive

strength) under displacement control following the protocol depicted in Fig. 5b. Two cycle increments were applied at each drift level in both directions according to FEMA 461 [33]. In particular, the increase of drift from cycle to cycle was 0.25 %, 0.50 %, 0.75 %, 1.0 %, 1.5 %, 2.0 %, 3.0 %, 4.0 %, 5.0 % (Fig. 5b).

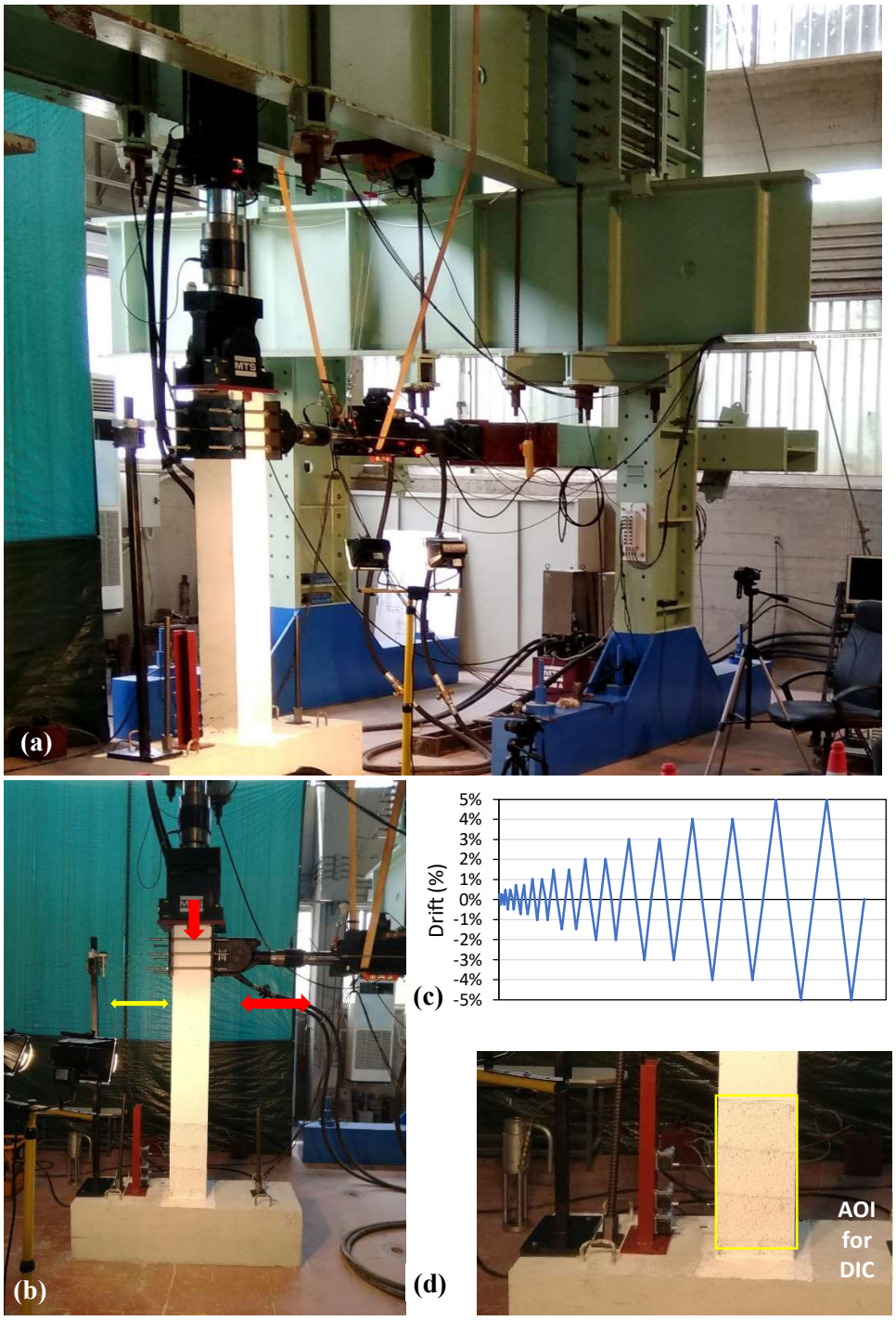

Fig. 5. (a) Test setup; (b) details of instrumentation; (c) Loading history; (c) Area of interest (AOI) for the DIC.

Digital Image Correlation (DIC) was used as an additional measurement technique and was applied on all four specimens by painting a speckle pattern on the area of interest (AOI), which extended 60cm from the column-footing connection. During testing, a DSLR camera captured high-resolution b/w images of the AOI at given drifts and these images were post-processed for producing strain contours of the principal tensile strain, ε_1, at 0.50, 0.75, 1.0, 1.5, 2.0, 3.0, 4.0 and 5.0% drift (Fig. 5c). The mean displacement confidence margin of the DIC setup was estimated at 1.2 μm.

2.5 Assessment of the as-built columns

The flexural strength at yielding, M_y, was calculated by performing cross-section analysis with Response 2000 software [34] for the four columns. The flexural shear strength, V_y, was calculated by using a shear span length equal to L_v = 1.64 m (Fig. 3). The cyclic shear resistance of the as-built columns was assessed by using Eurocode 8-Part 3 [35]:

$$V_{shear}^{EC8} = \frac{1}{\gamma_{el}} \cdot \left[\begin{array}{l} \frac{h-x}{2L_V} \cdot \min\left(N; 0.55 A_c f_c\right) + \left[1 - 0.05 \cdot \min(5; \mu_{\Delta,pl})\right] \cdot \\ \left[0.16 \cdot \max\left(0.5; 100\rho_{tot}\right) \left(1 - 0.16 \min\left(5; \frac{L_V}{h}\right)\right) \sqrt{f_c} \cdot A_c + V_w \right] \end{array} \right] \quad (1)$$

In Eq. (1), γ_{el} is equal to 1.15 for primary seismic elements (this is the case of the columns tested herein) and 1.0 for secondary seismic elements; h is the depth of cross-section; x is the compression zone depth; N is the compressive axial force (positive, taken as zero for tension); L_v is shear span length; A_c is the cross-section area; f_c is the concrete compressive strength; $\mu_{\Delta,pl}$ is the plastic displacement ductility (it was considered equal to zero as to calculate V_{shear}^{EC8} at yielding); ρ_{tot} is the total longitudinal reinforcement area; V_w is the contribution of transverse reinforcement to shear resistance. The results of M_y, V_y and V_{shear}^{EC8} for the as built columns (i.e. before the application of the SRG jackets for columns SRG1, SRG2, SRG3), presented in Table 4, indicate that all the columns had an inherent deficiency in shear.

As seen in Table 4, the shear strength ratio, $r_V=V_{shear}^{EC8}/V_y$ is lower than unity for all the specimens, hence shear cracking is expected to precede flexural yielding [36-39].

Table 4. Flexural and shear strength of the as-built columns.

Column	N (kN)	M_y (kNm)	V_y (kN)	x (mm)	V_{shear}^{EC8} (kN)	r_V
C	300	91	55.5	105.5	47.2	0.85
SRG1-as built	290	90	54.9	106.4	46.4	0.84
SRG2-as built	282	87	53.0	107.5	45.7	0.86
SRG3-as built	266	85	51.8	107.8	44.5	0.86

The chord rotation attained at yielding of longitudinal tension reinforcement, θ_y, is estimated by using the Eurocode 8-Part 3 [35] as follows:

$$\theta_y = \frac{1}{3}\varphi_y\left(L_V + \alpha_V \cdot z\right) + 0.0013\left(1 + 1.5\frac{h}{L_V}\right) + 0.13\varphi_y\frac{d_b f_y}{\sqrt{f_c}} \quad (2)$$

where φ_y is the yield curvature of the end section; L_v is the shear span length; $\alpha_v \cdot z$ represents the tension shift of the bending moment diagram [40], while $\alpha_v=1$ if shear cracking is expected to precede flexural yielding at the end of the member and z is the length of the internal lever arm; h is the section height; d_b denotes the mean diameter of the tension reinforcement; f_y and f_c are the steel yield stress and concrete strength (in MPa), respectively. The chord rotations at yielding for the as-built columns are given in Table 5.

Since shear cracking is expected to precede flexural yielding ($r_v < 1$), this will occur at a drift value [36-39]:

$$\theta_y^{shear} = r_v \cdot \theta_y \quad (3)$$

The plastic drift at ultimate, θ_u^{pl}, is calculated based on Eurocode 8-Part 3 [35]:

$$\theta_u^{pl} = 0.0185 \cdot \left(1 - 0.52\alpha_{cy}\right)\left(1 + \frac{\alpha_{sl}}{1.6}\right) \cdot (0.25)^v \left(\frac{\max\left(0.01, \omega'\right)}{\max\left(0.01, \omega\right)}\right)^{0.3} \cdot f_c^{0.2}\left(\frac{L_V}{h}\right)^{0.35} \cdot 25^{\left(\frac{\alpha_{st}\rho_{st}f_{y,st}}{f_c}\right)} \cdot 1.275^{100\rho_d} \quad (4)$$

In Eq. (4), α_{cy}=1 or 0 for cyclic or monotonic loading, respectively; α_{sl} = 1 or 0 if slippage of vertical bars from their anchorage past the column end is physically possible or not, respectively; ν is the dimensionless axial load; $\omega = \rho_{s1}f_y/f_c$ is the mechanical reinforcement ratio of the tension reinforcement (including any longitudinal reinforcement between the tension and the compression chord of the RC section); $\omega' = \rho_{s2}f_y/f_c$ is the mechanical reinforcement ratio of compression reinforcement; ρ_d is the ratio of diagonal reinforcement (if available in each diagonal direction); α_{st} is the confinement effectiveness factor; ρ_{st} is the ratio of transverse steel parallel to the direction of loading. All the other variables in Eq. (4) have already been defined. The calculated θ_y, θ_y^{shear}, θ_u^{pl}, and displacement ductility, $\mu_\Delta = 1+\theta_u^{pl}/\theta_y$, are presented in Table 5. The results indicate that if the columns could respond in a ductile way without any premature failure mode anticipated, the displacement ductility could reach a value of 2.

Table 5. Chord rotation at yielding and at ultimate.

Column	θ_y (%)	θ_y^{shear} (%)	θ_u^{pl} (%)	μ_Δ
C	2.26	1.92	2.47	2.1
SRG1-as built	2.29	1.93	2.46	2.1
SRG2-as built	2.32	2.00	2.44	2.1
SRG3-as built	2.34	2.01	2.42	2.0

Due to the sparse confinement reinforcement in the plastic hinge region of the columns, sideways buckling is the expected form of compression reinforcement failure due to lateral shear distortion of the member [9, 10]. The limiting strain ductility $\mu_{\varepsilon c} = \varepsilon_{s,crit}/\varepsilon_{sy}$ of the longitudinal bars in compression is plotted in Fig. 6 against the longitudinal bar diameter ratio (s/D_b) using the stress-strain law. The two curves correspond to different definitions considered for the modulus of elasticity, the tangent modulus, E_h [42], or the double modulus of elasticity, E_r [43]. For s/D_b = 15.6 the experimental value of the compressive strain ductility is $\mu_{\varepsilon c}$ = 1. This implies that the axial strain at which the bar becomes unstable, $\varepsilon_{s,crit}$, corresponds to the yielding strain of steel, $\varepsilon_{s,y}$.

The above assessment confirms that the as built columns have inherent deficiencies that will lead to a combination of shear and buckling failure. Shear cracks will dominate as soon as the column drift reaches a drift of $\theta_y^{shear} = 2\%$ (Table 5). At this drift level the compression reinforcement will start to yield and become unstable since $\mu_{\varepsilon c} = 1$.

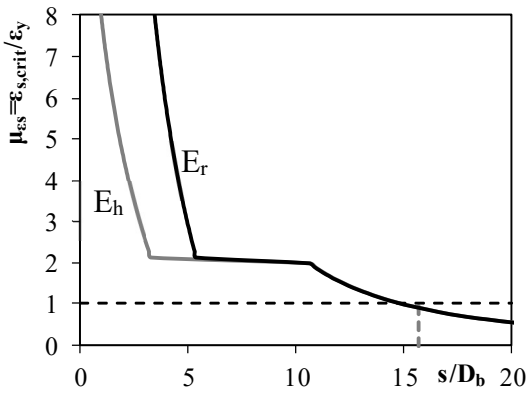

Fig. 6. Strain ductility, $\mu_{\varepsilon c}$, versus longitudinal bar diameter ratio, s/D_b

3. Experimental results and discussion

3.1 Damage assessment - Failure mechanisms

In this section, the damage evolution of the control and SRG jacketed columns with increasing drift is discussed with the help of the Digital Image Correlation (DIC) technique.

Control column: Upon the application of lateral load and at drift level equal to 0.25 %, the first crack formed at the control column – footing connection. More flexural cracks distributed at length equal to 60 cm from the column-footing connection (8-10 cm distance between the cracks, Fig. 7) appeared as the drift increased gradually to 1.0%. At 1.5% drift, the existing cracks became wider and the cracks evolved to flexural-shear cracks. The same crack pattern was observed at 2% drift with the shear cracks extending in the web of the cantilever. In addition, damage initiated at the compression reinforcement in the plastic hinge region (Fig. 7, drift +2.0%). This observation is in accordance with the assessment results where shear failure and compression reinforcement instability are expected at drift level $\theta_y^{shear} = 1.92$ % (Table 5).

The existing flexural and shear cracks became wider and the damage concentration was observed in the plastic hinge region due to bar buckling (Fig. 7, drift +3.0%). When the column entered the first 4% drift cycle, cracks parallel to the longitudinal reinforcement within the critical region appeared and the concrete cover of the column disintegrated. The reinforcing bars bent laterally to maintain compatibility with the increasing axial strain of the supporting concrete core. This is due to the fact that the sparse open stirrups (Ø6/250) could not provide sufficient confinement and thus a large unsupported length of the longitudinal reinforcing bars resulted. At the second 4% drift cycle, the stirrups at the first stirrup spacing opened and the bars buckled in the first two stirrups' spacing. The column collapsed at the beginning of the first cycle of 5% drift as seen in Fig. 7. As expected, the damage was concentrated in the first two stirrups' spacing (≈50cm). The state of the control cantilever at the end of the test is depicted in Fig. 8. The mode of failure observed is very common in old-type buildings.

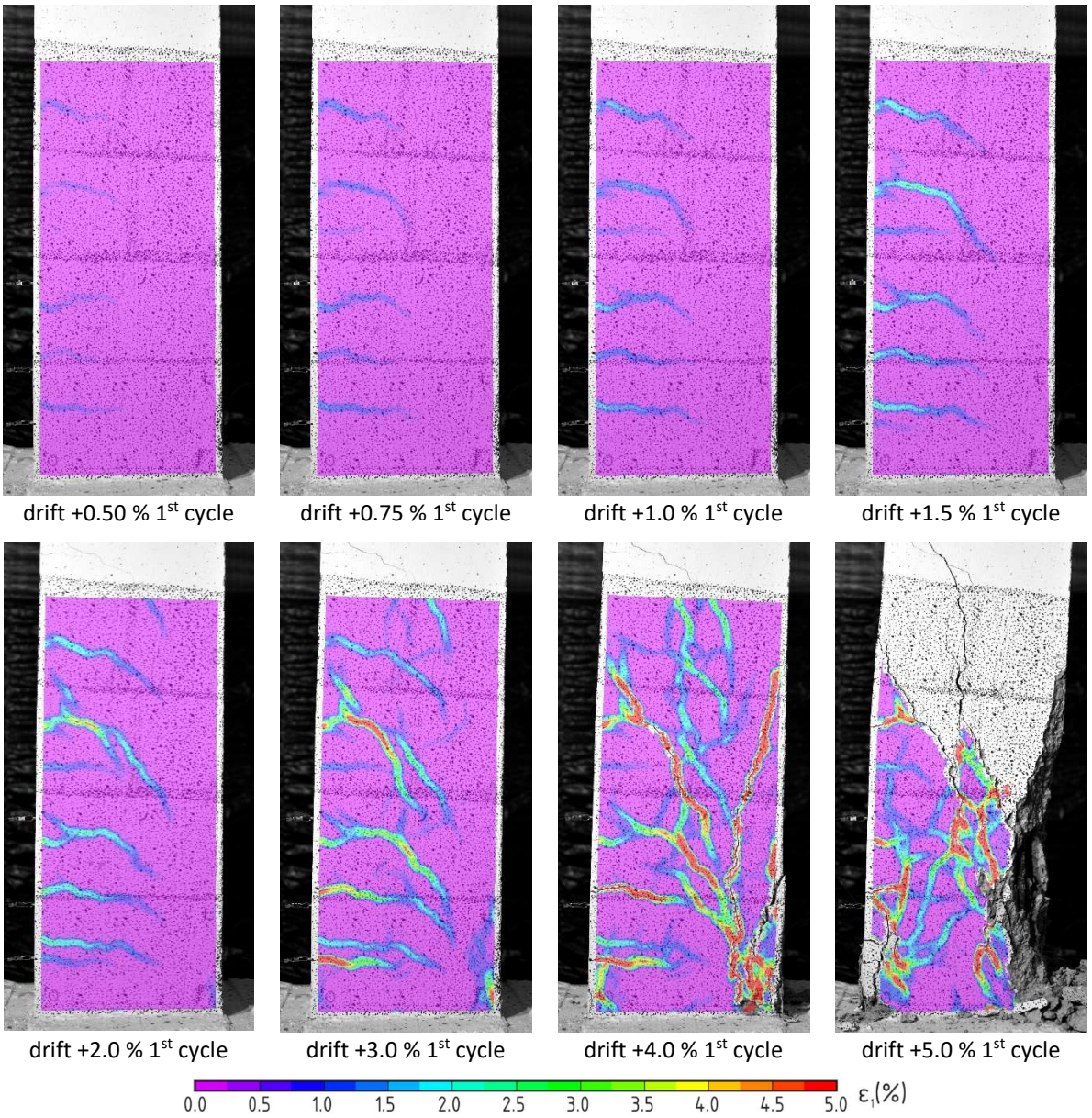

Fig. 7. DIC images for control C – principal tensile strain (ε_1) distribution at increasing drift.

Fig. 8. Evolution of damage in the control cantilever.

SRG jacketed columns: The evolution of damage with increasing drift for the three SRG jacketed cantilever columns is presented in Figs. 9-11. The addition of the SRG jackets modified substantially the response leading eventually to flexural failure. As observed in Figs. 9-11, the number of flexural cracks decreased as the number of layers and density of the textile increased. The SRG jackets remained intact until the end of the tests without observing any debonding or rupture of the textile. The state of the columns' critical region at the end of the tests is depicted in Figs. 12-14. The damage observed in the back-left corner of specimen SRG3 after removing the external layer of cracked mortar (shown in Fig. 14) is attributed to the difficulties in the application of the second layer of the textile as described in section "2.3 Fabrication of the SRG jackets".

After the removal of the steel textile in the critical region, the state of the concrete core of specimens SRG1, SRG2, SRG3 is presented in Fig. 15. The confinement provided even by a single layer of the 1.57 cords/cm density SRG jacket (i.e. SRG1) was enough to keep the concrete core in place and provide lateral support to the longitudinal reinforcement thus preventing sideways buckling of compression reinforcement. The removal of the textile was a difficult task due to the high level of bond developed between the textile and the mortar as well

as between the mortar and the concrete substate. There were cases that the textile had to be removed cord by cord, but the mortar remained attached to the concrete substate and cases that the removal of the textile was done in strips with the external layer of the concrete cover being attached to the mortar-textile system (Fig. 16).

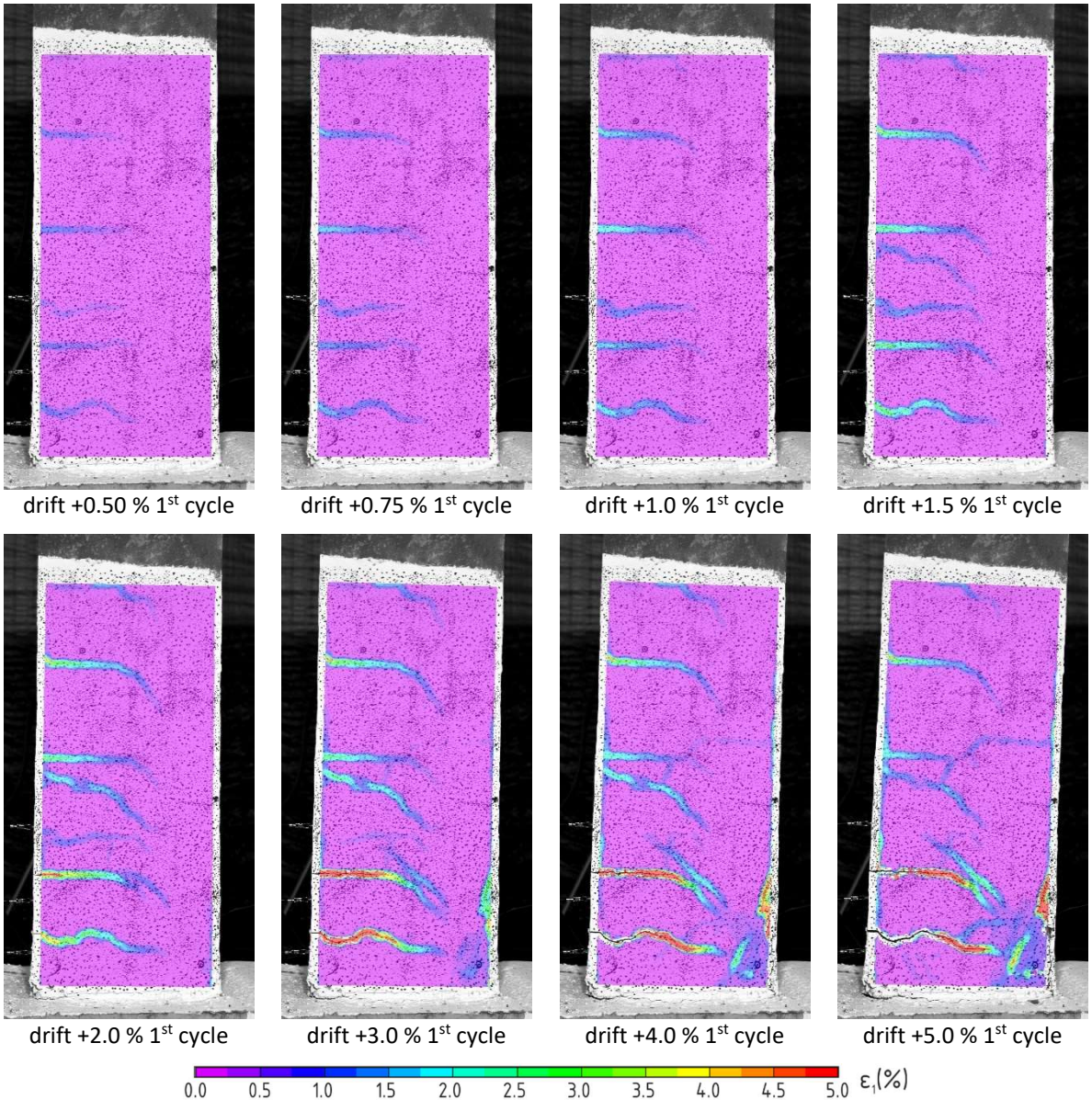

Fig. 9: DIC images for SRG1 (1 layer 1.57 cords/cm) – principal tensile strain (ε_1) distribution at increasing drift.

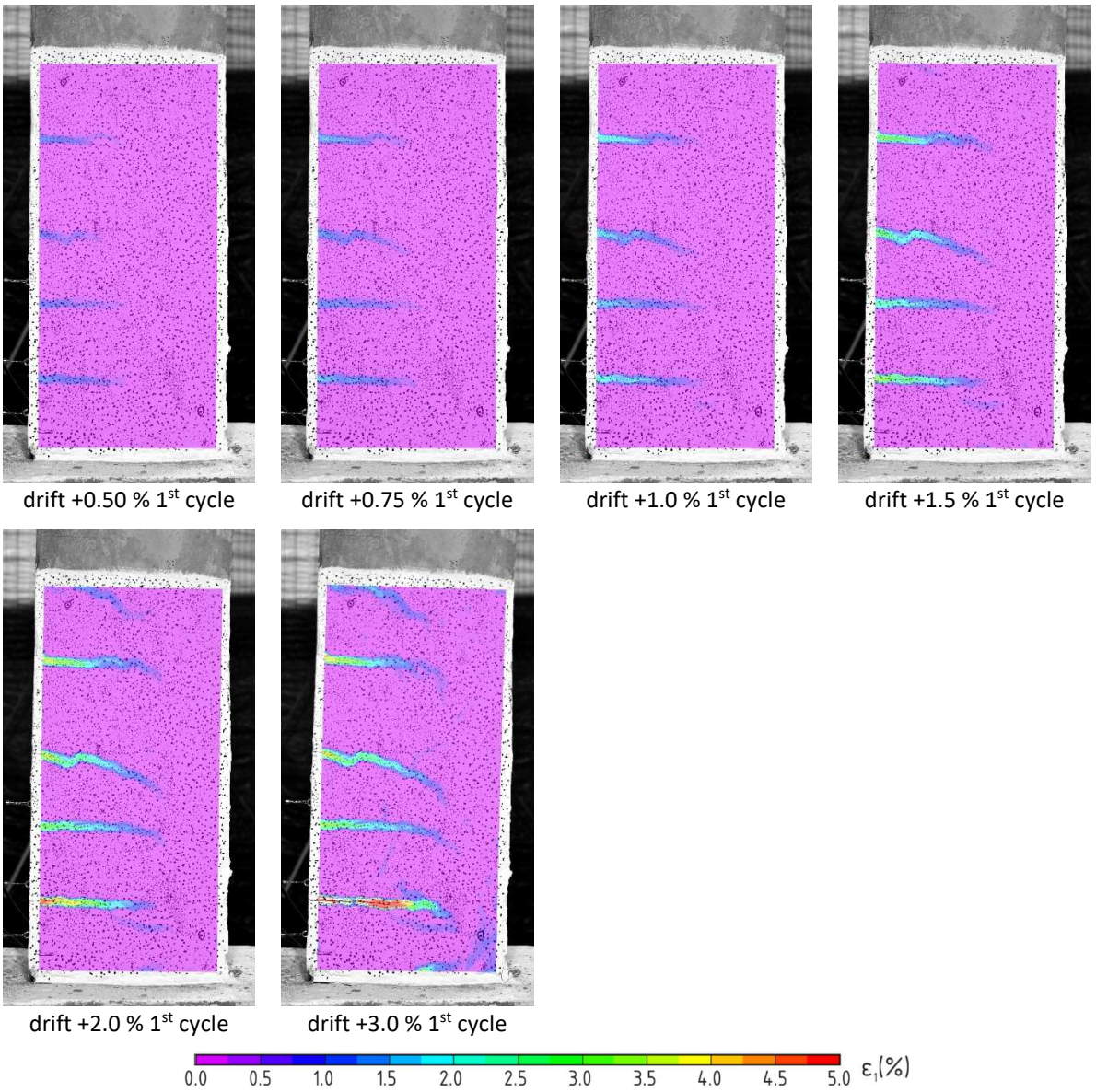

Fig. 10: DIC images for SRG2 (2 layers 1.57 cords/cm) – principal tensile strain (ε_1) distribution at increasing drift (note: no data for +4% and 5% due to technical difficulties).

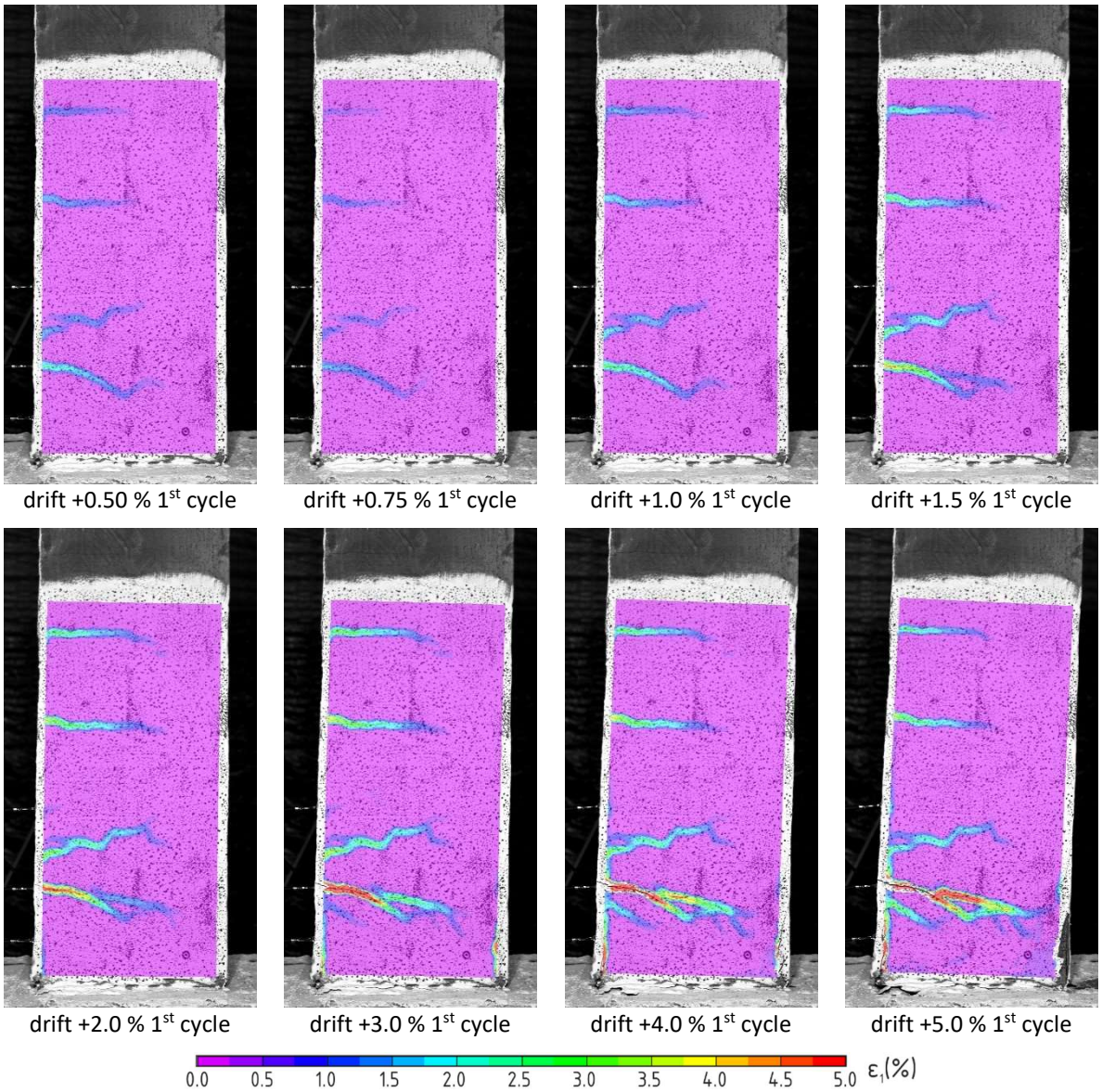

Fig. 11: DIC images for SRG3 (2 layers 4.72 cords/cm) – principal tensile strain (ε_1) distribution at increasing drift.

Fig. 12: Damage state at the end of the test for SRG1.

Fig. 13: Damage state at the end of the test for SRG2.

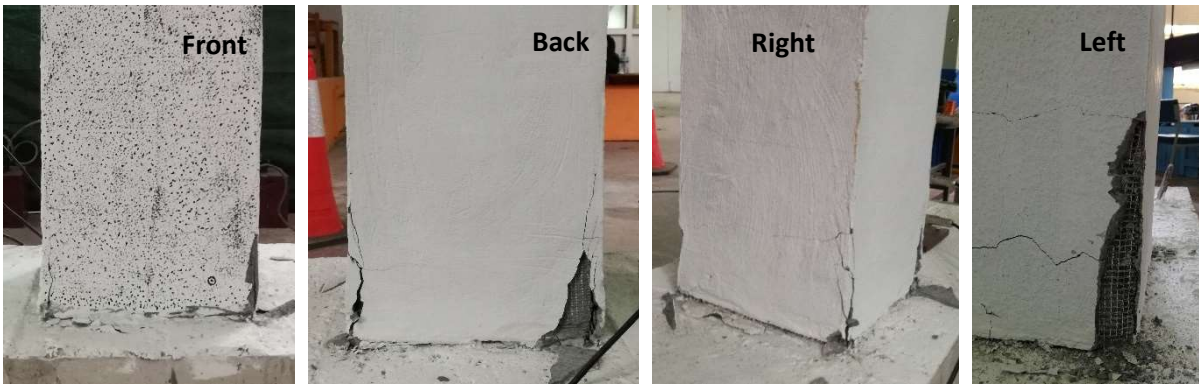

Fig. 14: Damage state at the end of the test for SRG3.

Fig. 15: State of the core cross section in the critical region after removal of the textile.

Fig. 16: State of the critical region after the removal of the textile.

3.2 Lateral load – drift hysteretic response

The test results are presented in Fig. 17 in the form of lateral load versus drift loops. The drift ratio is defined by dividing the tip deflection by the column's shear span length, L = 1640 mm (Fig. 2). The hysteretic curves were adjusted by considering the influence of P-Δ effects. A clear difference between the response of the control and the SRG jacketed columns can be observed in Fig. 18, where the envelope curves are compared. Table 6 presents the key test results such as the peak resistance, F_{max}, and the corresponding drift in the two directions of loading, θ_{max}, as well as the drift ratio at failure, θ_u (failure was defined by a 20% drop in lateral strength from the peak value).

The control specimen attained an average drift at failure of 3.9 %, whereas it collapsed at drift level 5 % (Fig. 7). The SRG1 column with a single layer of 1.57 cords/cm failed due to flexure at an average drift of 4.4%. The two-layered 1.57 cords/cm jacket applied in SRG2 column failed due to flexure at an average drift of 4.2 %. It is noted that during testing an unexpected interruption of the test of column SRG2 occurred at 2% drift level. The test continued from this drift level following the loading protocol previously described (Fig. 5b). Wrapping with two layers of the higher density textile (4.72 cords/cm) jacket led to flexural failure in column SRG3 occurred at an average drift level equal to 4.7 %. The peak resistance of the SRG jacketed columns was slightly increased (5 % average increase) compared to that of the control column (Table 6). Regarding the shear strength increase offered by the SRG

jackets, it ranged between 2-4 kN leading to the conclusion that SRG jacketing contributed mainly to increasing confinement.

From the above, it is concluded that the application of the SRG jackets managed to control the post peak behavior of the columns by displaying a gradual strength degradation. The longitudinal bars were protected from sideways buckling and the SRG jackets allowed the columns to reach an average drift level of 4.5 %, which is rather satisfying for RC columns with poor detailing subjected to seismic excitation. It should be noted that this drift capacity is beyond the 4% drift corresponding to Collapse Prevention (CP) performance level for concrete frames as suggested by ASCE/SEI 41-1 [38]. This indicates that in the scenario that these columns comprised the ground story columns of a building, they would have been protected from imminent collapse. The SRG jacketed columns at the end of the tests were considered repairable.

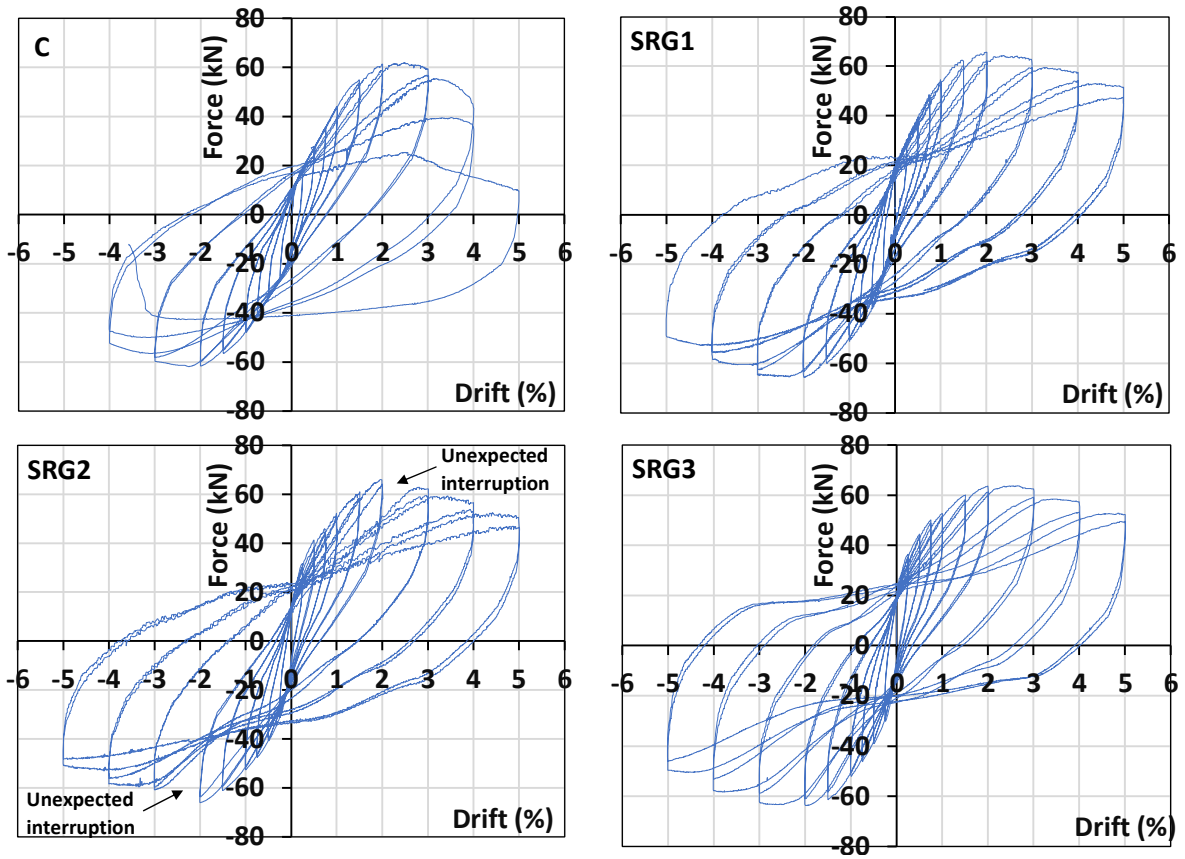

Fig. 17: Lateral force - drift hysteresis loops of the control and the SRG jacketed columns

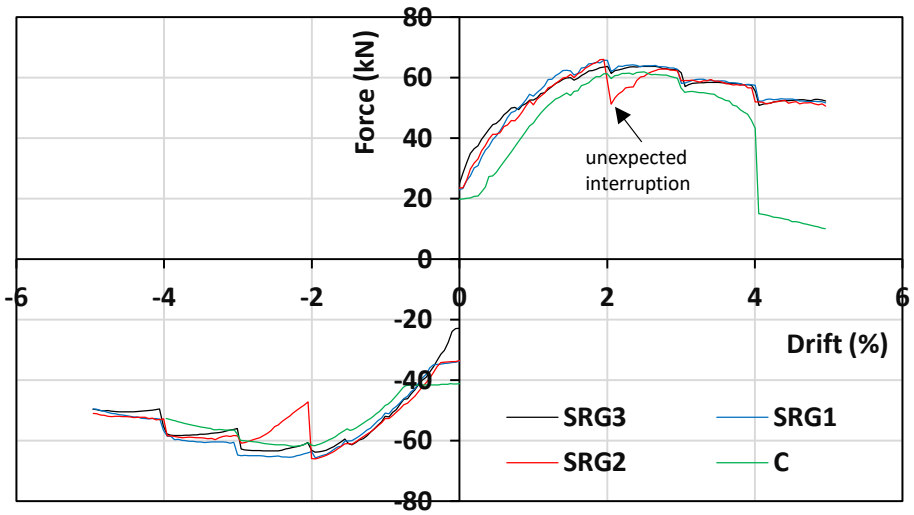

Fig. 18. Envelope curves of the control and the SRG jacketed columns.

Table 6. Test results.

Specimen	Peak Force, F_{max} (kN)		Drift at Peak Force, θ_{max} (%)		Ultimate Drift, θ_u (%)		Mode of failure
	Push	Pull	Push	Pull	Push	Pull	
C	61.84	-61.84	2.50	-2.24	3.80	-3.96	Shear/Buckling
SRG1	65.70	-65.70	2.00	-1.95	4.56	-4.31	Flexural
SRG2	65.99	-65.99	1.95	-1.95	4.00	-4.31	Flexural
SRG3	63.73	-63.73	2.66	-1.95	4.96	-4.51	Flexural

3.3 Axial expansion and shear strain in the plastic hinge region

The evolution of damage within the plastic hinge region is discussed in this section. The response of the control column C is compared to that of SRG3, which reached the maximum ultimate drift (Table 6). The length of the plastic hinge was $L_{pl} = 250$ mm (b in Fig. 19), calculated from the following expression [29]:

$$L_{pl} = \frac{L_v}{30} + 0.2h + 0.11\frac{d_{bl} f_y(\text{MPa})}{\sqrt{f_c(\text{MPa})}} \quad (5)$$

where L_v is shear span length; h is the depth of cross-section; d_{bl} is the diameter of tension reinforcement; f_y is the estimated mean value of steel yield strength; and f_c is the concrete compressive strength.

The mean vertical strain at center of cross section over 250 mm above the base (b = 250 mm in Fig. 19), ε_a, was measured by DIC. This value can represent the axial expansion within the

plastic hinge region. It can be seen that the mean vertical strain increases as the number and width of cracks within the region of interest increase and thus, it indirectly reflects the level of damage sustained within the critical region of the column. The axial expansion is plotted against the tip deflection in Figs. 20(a) and 20(c) for the control C and retrofitted SRG3 columns, respectively. Moreover, the evolution of axial expansion with increasing number of cycles is depicted in Fig. 20(e). Up to cycle 24, which corresponds to the second cycle of drift 2 % (yielding state), the control and the SRG jacketed columns present almost identical mean vertical strain values. For higher drift values (up to 4% drift for the control specimen, C), the axial expansion substantially increases for the control specimen due to the extensive crack patterns in the critical region (Fig. 7).

The shear strain in the critical region was derived by subtracting the two strain diagonals, ε_{d1} and ε_{d2} (shear strain: $\gamma = \varepsilon_{d1} - \varepsilon_{d2}$) measured in DIC (Fig. 19). The shear strain is plotted against the tip deflection in Figs. 20(b) and 20(d) for the control C and retrofitted SRG3 columns, respectively. The evolution of shear strain with the increasing cycles is also presented in Fig. 20(f). It can be seen that the passive confinement offered by the two-layered 4.72 cords/cm jackets substantially reduced the shear strain in SRG3 compared to the control column C. This finding clearly demonstrates the effectiveness of the SRG jacketing in modifying the response of deficient columns.

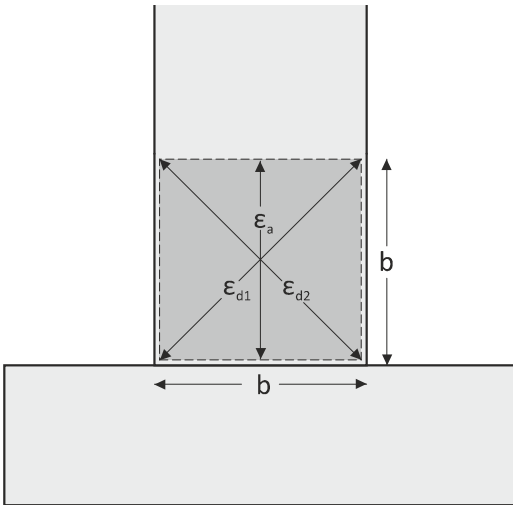

Fig. 19. Vertical strain in the middle of the cross section, ε_a, and strains in the diagonals, ε_{d1} and ε_{d2}, measured in DIC.

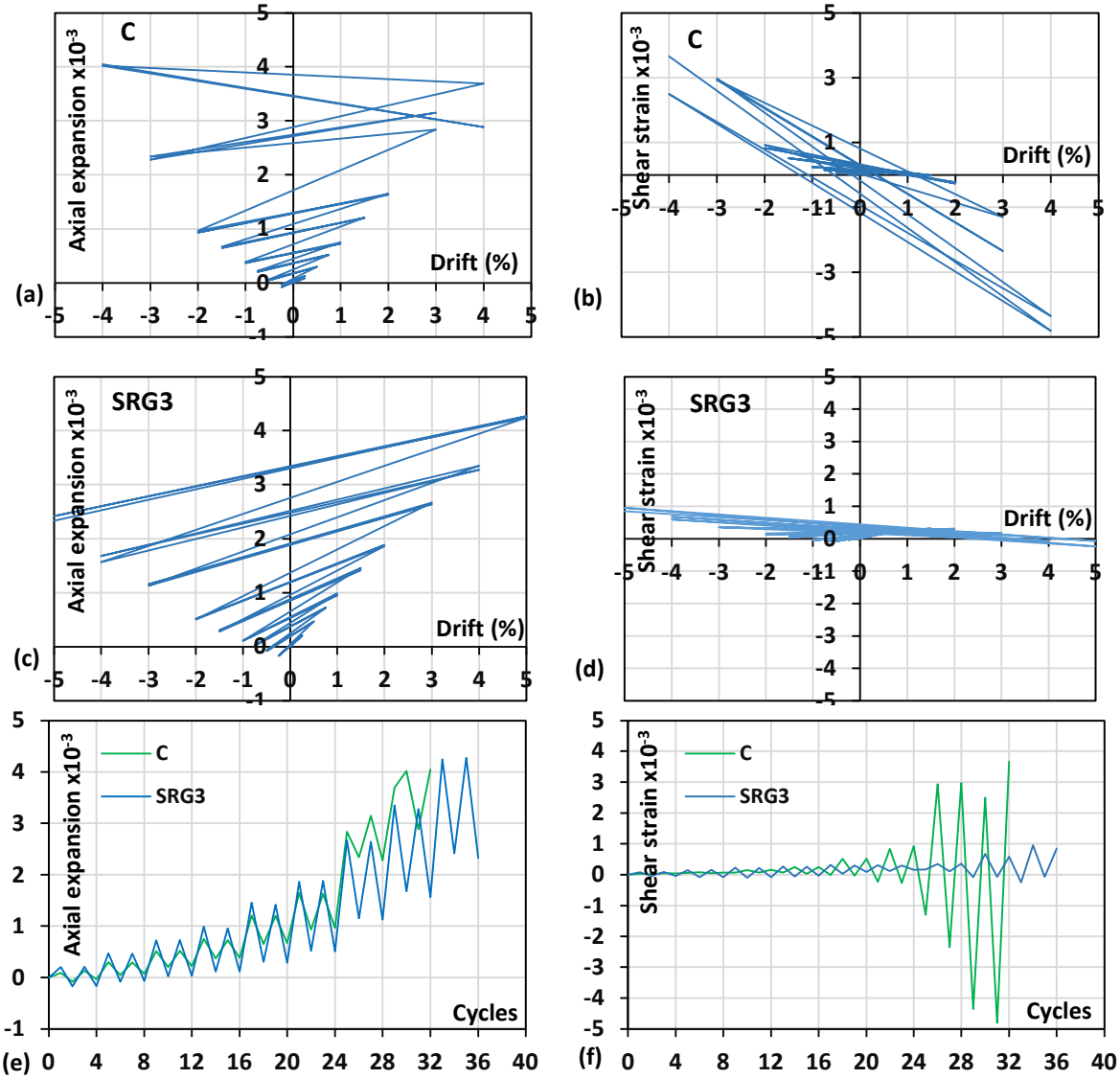

Fig. 20. Axial expansion and shear strain in the plastic hinge region for the control (C) and the SRG jacketed SRG3 column.

3.4 Hysteretic Energy

The dissipated energy per cycle as well as the cumulative dissipated energy (i.e. cumulative hysteretic area enclosed within the force-drift hysteresis loops presented in Fig. 17) are presented in Figs. 21(a) and 21(b), respectively. Since the control column C practically failed after the first cycle of 4% drift (Table 6), only the dissipated energy up to this cycle is considered in Fig. 21.

As observed in Fig. 21(a), the dissipated energy per cycle for the SRG jacketed columns was similar up to first cycle of 5%. In the last cycle (second cycle of 5%), the SRG2 (two-layered 1.57 cords/cm jacket) managed to dissipate 122 % and 16 % more energy than SRG1 (single-layered 1.57 cords/cm jacket) and SRG3 (two-layered 4.72 cords/cm jacket), respectively. Regarding the cumulative energy (Fig. 21(b)), SRG1, SRG2 and SRG3 dissipated 214 %, 234 % and 231 % more hysteretic energy compared to the control column C.

SRG1 jacketing was less efficient compared to SRG2 jacketing due to the lower geometric ratio of the steel textile (single- versus two-layered 1.57 cords/cm jacket). The difficulties related to the application of the second layer of the 4.72 cords/cm textile to specimen SRG3 (see section 2.3), rendered it equally efficient to SRG2 jacket in terms of dissipated energy (see Section 4 for further discussion).

From the above, the 1.57 cords/cm single-layered jacket applied to SRG1 proved to be quite efficient in modifying the response of the column from brittle to ductile and by dissipating only 8.5% less energy compared to the alternative SRG jacketing schemes with more layers and higher density textiles. Therefore, it can be considered as the most efficient intervention solution when both structural performance and construction costs are considered.

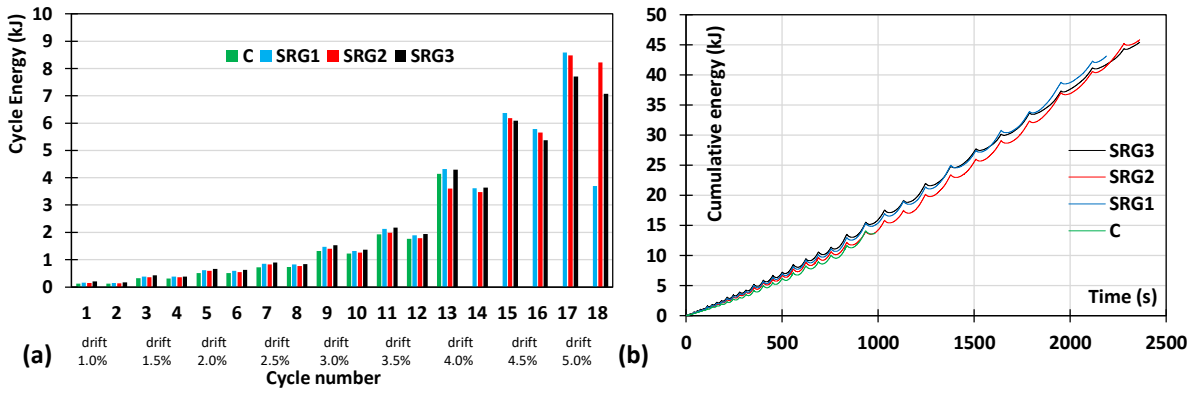

Fig. 21. (a) Dissipated energy per cycle; (b) Cumulative dissipated energy of the control and the SRG jacketed columns.

4. Assessing the performance of SRG jacketed columns using code formulations

The design philosophy presented in Chapter 8 of *fib* Bulletin 90 [8] for seismic retrofitting of existing substandard concrete structures using FRPs is implemented for the case of SRG jacketed columns tested herein to assess their strength and deformation capacity. The addition of SRG jackets to deficient RC columns aims to remove brittle failure modes, so that the flexural capacity may be fully developed and sustained up to a certain level of displacement ductility. For existing RC structures, $\mu_\Delta = 2.5$ is considered an achievable target displacement ductility [36, 45].

Confining pressure in SRG-encased concrete: Like FRP jacketing [8], the average confining pressure exerted by the SRG jacketing system when applied to RC members is obtained as the average lateral stress developing in the two principal directions of the cross section as:

$$\sigma_{lat} = \frac{1}{2}\underbrace{\left(\sigma_{SRG,lat,x} + \sigma_{SRG,lat,y}\right)}_{\text{SRG confinement}} + \frac{1}{2}\underbrace{\left(\sigma_{st,lat,x} + \sigma_{st,lat,y}\right)}_{\text{stirrup confinement}} = \frac{1}{2}\left(\underbrace{\alpha_{SRG}\cdot\rho_{v,SRG}\cdot E_{SRG}\cdot\varepsilon_{fu,h}}_{\text{SRG confinement}} + \underbrace{\alpha_{st}\cdot\rho_{v,st}\cdot f_{y,st}}_{\text{stirrup confinement}}\right) \quad (6)$$

where E_{SRG} is the modulus of elasticity and $\varepsilon_{fu,h}$ is the axial tensile strain of the SRG textile. The first and second part of Eq. (6) correspond to the contribution of the SRG jacket and stirrups, respectively. The subscripts x and y denote transverse pressure in the two principal directions of the cross section. $\rho_{v,SRG}$ and $\rho_{v,st}$ are the volumetric ratios of the SRG reinforcement and stirrups, respectively. The terms α_{SRG} and α_{st} are the confinement effectiveness factors for the SRG jacket and stirrup contribution, respectively. The term $\alpha_{st}(=\alpha_n\cdot\alpha_s)$ defined according to EC8-Part I [46] was estimated equal to 0.11 for the ∅6/250 stirrups. The low value of α^{st} indicates the negligible confinement effect of small bar diameter placed at sparse stirrup arrangement. The term a_{SRG} is defined as [8]:

$$\alpha_{SRG} = 1 - \frac{(b-2r)^2 + (h-2r)^2}{3A_g(1-\rho_l)} \quad (7)$$

where b, h are the width and height of the cross section, r is the corner radius, A_g is the cross sectional area and ρ_l is the percentage of the longitudinal reinforcement. The square columns (b=h) have sharp edges (r=0) and only one third of the cross section is well-confined, hence α_{SRG}=0.32. The calculated lateral confining pressure, σ_{lat}, for the SRG jacketed columns is presented in Table 7. $\varepsilon_{fu,h}$ is considered to be approximately 50% of the ultimate strain, ε_{fu}, of the cords [31].

The total lateral confining pressure exerted by the single layered 1.57 cords/cm jacket and the stirrups (∅6/250) is calculated equal to 0.19 MPa (see Table 7). Experimental evidence has demonstrated that this level of confining pressure was sufficient to allow column SRG1 to fail in a ductile manner. The second layer of 1.57 cords/cm density jacket in SRG2 column doubled the confining pressure exerted by the jacket compared to that of SRG1 column. While the higher lateral confining pressure did not increase the strength and deformation capacity any further, it contributed to reduce the number of flexural cracks and control damage within the critical region as discussed in section 3.1. Even though the confining pressure exerted by the higher density (4.72 cords/cm) jacket of SRG3 column is much higher when compared to that of SRG1 and SRG2 (Table 7), difficulties in the application of the second layer, as discussed in section 2.3, rendered this SRG jacketing configuration less effective than expected. The fact that the performance of SRG3 and SRG2 was very similar is confirmed by the cumulative energy results in Fig. 21(b), where the energy dissipated by SRG2 and SRG3 was 45.8 kJ and 45.4 kJ, respectively. Hence, is seems that the second 4.72 cords/cm layer of SRG3 jacket did not practically contribute to confinement.

Shear strength of SRG jacketed RC columns: The total shear strength of SRG jacketed RC columns, V_{shear}, comprises shear strength contributions from concrete and steel stirrups, V_{shear}^{EC8} (Eq. (1)), and SRG jacket, V_{SRG}:

$$V_{shear} = V_{shear}^{EC8} + V_{SRG} \leq V_{Rd,max} \quad (8)$$

where $V_{Rd,max}$ is the maximum shear resistance defined according EC2-Part I [34] as calculated in Table 6. V_{shear}^{EC8} is presented in Table 4. The shear strength contribution from the SRG jacket is [47]:

$$V_{SRG} = n \cdot \rho_{SRG} \cdot b \cdot d \cdot \varepsilon_{SRG,eff} \cdot E_{SRG} \quad (9)$$

where n is the number of textile layers applied; ρ_{SRG} (=2·t_{SRG}/b) is the SRG geometric ratio for a single layer; h and d are the height and the effective depth of the cross section, respectively. In Eq. (9), the effective strain, $\varepsilon_{SRG,eff}$, corresponds to a fraction of the rupture strain for the cords, ε_{fu}, and is used to account for the reduction of SRG strength due to bending of the fibers at the corners of the cross section. In this study, $\varepsilon_{f,eff}$ was considered to be approximately 50% of the ultimate strain, ε_{fu}, of the cords [47].

The shear strength contribution of the three SRG jacketing configurations, $V_{SRG,}$ is presented in Table 7. The total shear strength capacity of the SRG jacketed RC columns, V_{shear}, is higher than the flexural shear strength of the as built columns, V_y ($V_{shear} > V_y$) (Tables 4 & 7). This implies that the SRG jackets are efficient at increasing the inherent shear strength. Even in the case of the lowest density single-layered jacket (1.57 cords/cm, SRG1), brittle failure can be removed as confirmed by experimental evidence.

Table 7. Properties of the SRG jacketed columns.

Column	Type of jacket	σ_{lat} (MPa)	V_{SRG} (kN)	V_{shear} (kN)	$V_{Rd,max}$ (kN)	θ_y (%)	$\theta_{u,SRG}^{pl}$ (%)	$\theta_{u,SRG}$ (%)	$\mu_{\Delta,SRG}$
SRG1	1 layer 1.57 cords/cm	0.19	58.8	105.2	511.4	2.29	2.57	4.69	2.1
SRG2	2 layers 1.57 cords/cm	0.34	117.6	163.3	499.5	2.32	2.67	4.83	2.2
SRG3	2 layer 4.72 cords/cm	0.94	355.6	400.1	473.5	2.34	3.22	5.40	2.4

Chord rotation at yielding and ultimate: The chord rotation at yielding of the SRG jacketed columns is considered to remain the same as that of the as-built column (Eq. (2), θ_y in Tables 5 & 7). The plastic part of the ultimate chord rotation of the SRG jacketed columns, $\theta_{u,SRG}^{pl}$, is calculated based on the empirical model suggested for FRP-jacketed members [35, 41]:

$$\theta_{u,SRG}^{pl} = 0.0185 \cdot \left(1 - 0.52\alpha_{cy}\right)\left(1 + \frac{\alpha_{sl}}{1.6}\right) \cdot (0.25)^{v} \left(\frac{\max\left(0.01, \omega'\right)}{\max\left(0.01, \omega\right)}\right)^{0.3} \cdot f_c^{0.2} \left(\frac{L_s}{h}\right)^{0.35} \cdot 25^{\left(\frac{\alpha_{st}\rho_{st}f_{y,st}}{f_c} + \beta\right)} \cdot 1.275^{100\rho_d} \quad (10)$$

Eq. (10) is similar to Eq. (4) apart from term β, which in the original expression suggested by Biskinis and Fardis [41] reflects the confinement by FRP jacketing, whereas here it reflects the confinement by SRG jacketing:

$$\beta = \frac{\alpha_{SRG} n \cdot \rho_{SRG} \varepsilon_{SRG,eff} E_{SRG}}{f_c} \quad (11)$$

The displacement ductility provided by the SRG jacketed members is defined as:

$$\mu_{\Delta,SRG} = 1 + \frac{\theta_{u,SRG}^{pl}}{\theta_y} \quad (12)$$

The predicted values of the plastic part of the chord rotation capacity, $\theta_{u,SRG}^{pl}$, displacement ductility, $\mu_{\Delta,SRG}$, and ultimate chord rotation, $\theta_{u,SRG}$, are presented in Table 7. The comparison between the predicted $\theta_{u,SRG}$, and the experimental θ_u (Table 6) yields that Eurocode 8-based formulation (Eq. (10)), if used for SRG jacketed columns, overestimates the ultimate chord rotation capacity by 8% on average.

Buckling: The bar slenderness ratio of compression reinforcing bars supported laterally by stirrups for the columns of this test campaign is $\lambda = s/D_b = 250/16 = 15.6$. As mentioned before, for $\lambda > 10$ the bar may undergo elastic buckling prior to yielding [8]. The effectiveness of the SRG jacket as lateral support to longitudinal reinforcement is limited by the stress concentrations when the bars reach conditions of instability at the critical axial strain, $\varepsilon_{s,crit}$. SRG jacketing should provide enough lateral restraint so that the stain capacity of confined concrete, $\varepsilon_{cu,c}$, exceeds the critical strain, $\varepsilon_{s,crit}$, at the onset of reinforcement buckling.

Following the methodology suggested in *fib* bulletin 90 [8], for a target displacement ductility, $\mu_{\Delta,req} = 2.5$, the curvature ductility demand is calculated per $\mu_{\varphi,req} = 2\mu_{\Delta,req} - 1 = 4$. The corresponding required concrete compression strain is:

$$\varepsilon_{cu,c}^{req} = 2.2\mu_{\phi,req} \cdot \varepsilon_{sy} \cdot \nu \geq 0.0035 \quad (13)$$

$\varepsilon_{cu,c}^{req}$ is defined equal to $2.2 \cdot 4 \cdot 550/200000 \cdot 0.2 = 0.0048 > 0.0035$. The SRG jacket should ensure a required strain $\varepsilon_{cu,c} \geq \max(\varepsilon_{cu,c}^{req}, \varepsilon_{s,crit})$ ($\varepsilon_{s,crit}$ was defined in section "2.5 Assessment of the as-built columns"). The ultimate strain of SRG confined members, $\varepsilon_{cu,c}$, is then defined by [25]:

$$\varepsilon_{cu,c}/\varepsilon_{co} = 1.75 + 32.78 \cdot \rho_K \cdot \rho_\varepsilon \quad \text{where} \quad \rho_\varepsilon = \frac{\varepsilon_{SRG,eff}}{\varepsilon_{co}}; \rho_k = \frac{1}{2}\frac{\rho_{v,SRG} E_{SRG} \varepsilon_{co}}{f_{co}} \quad (14)$$

In the above equation, ε_{co} is the strain corresponding to the peak compressive strength of unconfined concrete; and f_{co} is the compressive strength of the unconfined concrete (here the average of the as-built SRG1, 2, and 3 was considered).

The volumetric ratio of the SRG jacket, $\rho_{v,SRG}$, is calculated equal to 0.064 % for $\varepsilon_{cu,c}$=0.0048. The required total thickness for the SRG jacket is t_f = 0.04 mm. This corresponds practically to one layer of 1.57 and 4.72 cords/cm density textiles.

As discussed above, a single-layered jacket with 1.57 cords/cm density is considered sufficient to remove brittle failure modes and delay bar buckling for a target displacement ductility equal to $\mu_{\Delta,req}$=2.5. Experimental evidence has demonstrated that a single layer of SRG was adequate to prevent brittle failure of the columns.

5. Conclusions

An experimental investigation was carried out to study the efficiency of SRG jackets in modifying the response of substandard, full scale cantilever RC columns subjected to combined axial loading and cyclic lateral displacement reversals. Four column specimens were constructed following the construction practice of the 1970s in southern Europe with a bar slenderness ratio of $s/D_b = 15.6$. All the columns were designed to be susceptible to sideways bar buckling, a typical mode of failure in existing substandard buildings designed without considering any seismic code provisions. Alternative SRG jacketing schemes differentiated per the density of the fabric (1.57 and 4.72 cords/cm) and the number of layers (one and two layers for the 1.57 cords/cm fabric and two layers for the 4.72 cords/cm fabric) were used to strengthen the other three full-scale columns. The SRG strengthened columns were subjected to combined axial loading and cyclic lateral displacement reversals. The conclusions drawn from this study are summarized as follows:

1. The density of Ultra-High Tensile Strength Steel (UHTSS) textiles is a determinant parameter for the successful application of the SRG jacketing system. Textiles with density as high as 4.72 cords/cm, even if they are pre-bent, can be very difficult to apply, especially in the case than more than one layers are required. Based on the results of current study and previous research [19, 21-24], it is advised textiles with a density up to 3.15 cords/cm to be used for jacketing. In the case that higher densities are selected (not higher than 4.72 cords/in), single-layered jackets should be applied.
2. The control column failed due to buckling at an average drift of 3.9 % verifying that the sparse open stirrups (Ø6/250) could not provide the required lateral support to the longitudinal reinforcing bars. The mode of failure observed is typical for buildings with old-type detailing.

3. The application of the SRG jackets substantially modified the failure mode of the columns from brittle to flexural. SRG jacketing controlled the column post peak behavior by displaying a gradual strength degradation. The SRG jacketed columns reached an average drift at failure of 4.5 % corresponding to a displacement ductility of 2.5, which is considered achievable for retrofitted buildings with inherent deficiencies. The highest drift at failure was attained by the SRG3 column corresponding to 5 %. SRG jacketing had a slight impact (an average value of 5 % increase) on the ultimate strength of the strengthened columns.
4. The SRG jacketed columns dissipated on average 226 % more hysteretic energy compared to the control column C. The energy dissipated by SRG1 column (single-layered 1.57 cords/cm jacket) was only 6% lower compared to SRG2 (two-layered 1.57 cords/cm jacket) and SRG3 (two-layered 4.72 cords/cm jacket) columns, despite the significantly lower lateral confining pressure exerted by the SRG1 jacket. The higher lateral confining pressure exerted by the two-layered 1.57 cords/cm jacket in SRG2 led to a smaller number of flexural cracks and more controlled damaged within the critical regions compared to SRG1. However, it did not increase further the strength and deformation capacity of the column. In case of the two layered 4.72 cords/cm jacketed column (SRG3), the second layer seems to have negligible contribution to the confinement of the column due to construction defects, thus rendering the jacketing system less efficient. In terms of the cumulative energy, the two layered 1.57 and 4.72 cords/cm jackets were equally efficient.
5. One layer of the lower density textile (1.57 cords/cm) managed to suppress the premature failure mode and to provide adequate confinement and lateral support to the longitudinal reinforcement, thus preventing sideways buckling of compression reinforcement. The adequacy of one layer of 1.57 cords/cm (4 cords/in) density textile was confirmed by the code formulations.

Acknowledgments

The experimental program was conducted in the Laboratory of Reinforced Concrete and Masonry Structures, School of Civil Engineering, Aristotle University of Thessaloniki. Special thanks are attributed to Kerakoll S.p.A. for providing the Ultra High Tensile Strength Steel (UHTSS) textiles and mortar. This project has received funding from the European Union's Horizon 2020 research and innovation programme under the Marie Skłodowska-Curie grant agreement No. 700863.

References

[1]Thermou, G.E. (2014) "Strengthened Structural Members and Structures: Analytical Assessment" Encyclopedia of Earthquake Engineering edited by Michael Beer, Edoardo Patelli, Ioannis Kougioumtzoglou and Ivan Siu-Kui Au, www.SpringerReference.com.

[2]fib bulletin 24 (2003). "Seismic assessment and retrofit of reinforced concrete buildings." State of the art report, Task Group 7.1, fédération internationale du béton (fib).

[3]Mau, S. Effect of tie spacing on inelastic buckling of reinforcing bars. ACI Structural Journal, 1990;87(6):671-677.

[4]Monti G, Nuti C. Nonlinear cyclic behavior of reinforcing bars including buckling. J Struct Eng 1992;118(12):3268-3284.

[5]Pantazopoulou S. Detailing for reinforcement stability in RC members. J Struct Eng 1998;124(6):623-632.

[6]Yalcin C, Saatcioglu M. Inelastic analysis of reinforced concrete columns. Comp Struct 2000;77:539-555.

[7]Pantazopoulou SJ, Tastani SP, Thermou GE, Triantafillou T, Monti G, Bournas D Guadagnini M. Background to European seismic design provisions for the retrofit of R.C. elements using FRP materials. Fib Struct Concr J 2016;17(2):133–305.

[8]fib bulletin 90 (2019). "Externally applied FRP reinforcement for concrete structures." Technical report, Task Group 5.1, fédération internationale du béton (fib).

[9]Tastani S, Pantazopoulou S, Zdoumba D, Plakantaras V, Akritidis E. Limitations of FRP jacketing in confining old-type reinforced concrete members in axial compression. J Compos Constr 2006;10(1):13-25.

[10] Tastani S, Pantazopoulou S. Detailing procedures for seismic rehabilitation of reinforced concrete members with fiber reinforced polymers. Eng Struct 2008;30(2):450-461.

[11] Pantelides, C.P., Duffin, J.B., Reaveley, L.D. (2007). Seismic strengthening of reinforced-concrete multicolumn bridge piers, Earthquake Spectra, 23(3), pp. 635-664

[12] Thermou GE, and Pantazopoulou SJ. Fiber reinforced polymer retrofitting of substandard RC prismatic members. J Compos Constr 2009;13(6):535-546.

[13] Ilki, A., Demir, C., Bedirhanoglu, I., Kumbasar, N. (2009) Seismic retrofit of brittle and low strength RC columns using fiber reinforced polymer and cementitious composites, Advances in Structural Engineering, 12(3), pp. 325-347

[14] Garcia R, Hajirasouliha I & Pilakoutas K (2010) Seismic behaviour of deficient RC frames strengthened with CFRP composites. Engineering Structures, 32(10), 3075-3085.

[15] Lin, G., Zeng, J.J., Teng, J.G., Li, L.J. (2020). Behavior of large-scale FRP-confined rectangular RC columns under eccentric compression, Engineering Structures, 216,110759

[16] Bournas DA, Lontou PV, Papanicolaou CG, Triantafillou TC. Textile-Reinforced Mortar versus Fiber-Reinforced Polymer Confinement in Reinforced Concrete Columns. ACI Struct J 2007;104(6):740-748.

[17] Bournas DA, and Triantafillou TC. Bar buckling in RC columns confined with composite materials. J Compos Constr 2011; 15(3):393-403.

[18] Park, S.-H., Dinh, N.H., Um, J.-W., Choi, K.-K. (2021). Experimental study on the seismic performance of RC columns retrofitted by lap-spliced textile-reinforced mortar jackets after high-temperature exposure, Composite Structures, 256, Article: 113108.

[19] Garcia R, Pilakoutas K, Hajirasouliha I, Guadagnini M, Kyriakides N & Ciupala MA (2017) Seismic retrofitting of RC buildings using CFRP and post-tensioned metal straps: shake table tests. Bulletin of Earthquake Engineering, 15(8), 3321-3347.

[20] Kazemi, M.T., Morshed, R. (2015) “Seismic shear strengthening of R/C columns with ferrocement jacket” Cement and Concrete Composites, 27(7-8), 834-842.

[21] Manaha, Y.P., Suprobo, P., Faimun (2020) “Behavior of reinforced concrete columns retrofitted by welded wire mesh jackets” International Journal of Advanced Science and Technology, 29(8 Special Issue), 884-896.

[22] Shin, M. Bassem A. (2011) “Lateral cyclic behavior of reinforced concrete columns retrofitted with shape memory spirals and FRP wraps” ASCE Journal of Structural Engineering, 137(11), 1282-1290.

[23] Gholampour, A., Hassanli, R., Mills, J.E., Vincent, T., Kunieda, M. (2019) "Experimental investigation of the performance of concrete columns strengthened with fiber reinforced concrete jacket" Construction and Building Materials, 194, 51-61.

[24] Ali Dadvar S., Mostofinejad D., Bahmani H. (2020) "Strengthening of RC columns by ultra-high performance fiber reinforced concrete (UHPFRC) jacketing" Construction and Building Materials, 235, 117485.

[25] Fantilli, A.P., Meloni, L.P., Nishiwaki, T., Igarashi, G. (2019) "Tailoring confining jacket for concrete column using ultra high performance-fiber reinforced cementitious composites (UHP-FRCC) with high volume fly ash (HVFA)" Materials, 12(23), 4010.

[26] Thermou GE, Pantazopoulou SJ. Metallic fabric jackets: an innovative method for seismic retrofitting of substandard RC prismatic members. Fib Struct Concr J 2007;8(1):35-46.

[27] Thermou, G.E., Katakalos, K. and Manos, G. (2018) "Experimental investigation of substandard RC columns confined with SRG jackets under compression" Composite Structures, 184, 55-65.

[28] Royal Decree (1959). Earthquake design regulation of building works. Royal Decree (19/26.02.1959), Ministry of Public Works, Greece (in Greek).

[29] Thermou GE, Katakalos K and Manos G. Concrete confinement with steel-reinforced grout jackets. Mater Struct 2015;48(5):1355-1376.

[30] Thermou GE, Katakalos K, Manos G. Influence of the cross section shape on the behavior of SRG-confined prismatic concrete specimens. Mater Struct 2016;49(3):869-887.

[31] Thermou, G.E., and Hajirasouliha, I. (2018) "Design-oriented models for concrete columns confined by steel-reinforced grout jackets" Construction and Building Materials, 178, 313-326. 2.

[32] Thermou, G.E., and Hajirasouliha, I. (2018) "Compressive behavior of concrete columns confined with steel-reinforced grout jackets" Composites Part B: Engineering Journal, 138, 222-23.

[33] FEMA 461 (2007). Interim testing protocols for determining the seismic performance characteristics of structural and non-structural components, Applied Technology Council, Redwood City, CA, 113 pp.

[34] Bentz EC, Collins MP. Response – 2000. Reinforced concrete sectional analysis nusing the modified compression field theory, Toronto; 2000.

[35] EN 1998-3 (2005), Eurocode 8: Design of structures for earthquake resistance - Part 3: Assessment and retrofitting of buildings, European Committee for Standardization (CEN), Brussels.

[36] Thermou, G.E, Elnashai, A.S., and Pantazopoulou, S.J. (2010) "Design and assessment spectra for retrofitting of RC buildings." Journal of Earthquake Engineering, 14 (5), 743-770.

[37] Thermou, G.E., and Pantazopoulou, S.J. (2011) "Assessment indices for the seismic vulnerability of existing RC buildings." Journal of Earthquake Engineering and Structural Dynamics, 40 (3), 293-313.

[38] Thermou, G.E., Pantazopoulou, S.J., and Elnashai, A.S. (2012) "Global interventions for seismic upgrading of substandard RC buildings." Journal of Structural Engineering, ASCE, 138(3), 387-401.

[39] Pardalopoulos, S.J., Thermou, G.E., and Pantazopoulou, S.J. (2013). "Screening Criteria to Identify Brittle RC Structural Failures in Earthquakes." Bulletin of Earthquake Engineering, 11(2), 607–636.

[40] EN 1992-1-1 (2004), Eurocode 2. Design of concrete structures – Part 1-1: General rules and rules for buildings, European Committee for Standardization (CEN), Brussels.

[41] Biskinis, D., Fardis, M.N. (2013). Models for FRP-wrapped rectangular RC columns with continuous or lap-spliced bars under cyclic lateral loading, Engineering Structures, 57, pp. 199-212.

[42] Priestley M, Seible F, Calvi M. Seismic design and retrofit of bridges. New York: Wiley; 1996.

[43] Papia M, Russo G, Zingone G. Instability of longitudinal bars in RC columns. J. Struct. Eng 1988;114(2):445–61.

[44] ASCE/SEI 41-17 (2017) Seismic Evaluation and Retrofit of Existing Buildings, Standard, merican Society of Civil Engineers, 550p.

[45] Thermou, G.E., Pantazopoulou, S.J., and Elnashai, A.S. (2007) "Design methodology for seismic upgrading of substandard RC structures." Journal of Earthquake Engineering, 11 (4), 582-606.

[46] EN 1998-1-1 (2004), Eurocode 2. Design of concrete structures – Part 1-1: General rules and rules for buildings, European Committee for Standardization (CEN), Brussels.

[47] Thermou, G.E., Papanikolaou, V.K., Lioupis, C., Hajirasouliha, I. (2019) Steel-Reinforced Grout (SRG) strengthening of shear-critical RC Construction and Building Materials 216, pp. 68-83